



ELSEVIER

29 May 2000

PHYSICS LETTERS A

Physics Letters A 270 (2000) 149–156

www.elsevier.nl/locate/pla

Effects of rotation on fronts of density currents

A. Mahalov^{a,*}, J.R. Pacheco^a, S.I. Voropayev^a, H.J.S. Fernando^a, J.C.R. Hunt^b^a Arizona State University, Tempe, AZ 85287-9809, USA^b Department of Space and Climate Physics, University College London, W.C.1, London, UK

Received 15 September 1999; received in revised form 4 April 2000; accepted 11 April 2000

Communicated by C.R. Doering

Abstract

The effects of background rotation with angular velocity $f/2$ are studied for buoyancy driven currents of initial height h_0 whose density exceeds by $\Delta\rho$ the ambient value of ρ_0 . Our aim is to find how viscous density currents adjust in time under effects of background rotation focusing on time evolution of fronts of density currents. Rotation reduces the front velocity, $U_F^f = F(ft)U_F^0$, of the density current which is compared to a non-rotating case, U_F^0 , by the function $F(ft)$ where $F \rightarrow 1$ as $ft \rightarrow 0$ and $F \rightarrow 0$ as $ft \rightarrow \infty$. When the parameter $\mu = ft$ becomes of order one, there is a transition to the geostrophic asymptotic regime. We present numerical results for the transition curve for the density current front radial position for axisymmetric density currents on a rigid surface in a rotating frame. The transition is from a non-rotating power law to a long-time solution. The results of laboratory experiments are found to agree with the results of numerical simulations. © 2000 Published by Elsevier Science B.V. All rights reserved.

Keywords: Nonlinear dynamics; Rotation; Density currents; Scaling laws

1. Introduction

A characteristic feature of many types of geophysical flows on a wide variety of length and time scales are sloping interfaces separating zones of less dense and more dense fluid [1]. Because long waves on stable layers of fluid tend to travel faster the deeper the layer, it means that fluid from the deep part of the zone tends to move towards the shallower leading edge of the zone. This process tends to increase

or maintain high gradients of density at the boundary, which becomes a sharply defined interface. The higher hydrostatic pressure at the base of the zone of dense fluid forces it to move into the lower part of the zone of less dense fluid, producing the well-known phenomena of natural gravity currents [2]. Even when the currents are unsteady and are generated by different geophysical causes, they may have the same form of front. However, there are also situations where differing dynamical forces operate to produce significant variability in the form of the front.

On the mesoscale (say less than 10 km in the atmosphere), there might be external shear flows opposing the fronts' movement [3] or strong exter-

* Corresponding author. Tel. +1-480-965-3951; fax: +1-480-965-8119.

E-mail address: alex@taylor.la.asu.edu (A. Mahalov).

nally produced mixing [4]. On larger meso-synoptic scales, the main disturbing factor is the Earth's rotation, with the angular velocity $f/2$, which tends to bring the movement of the front to a standstill. In this case the front develops into a wedge-like 'geostrophic front', which differs from a gravity current in that there are significant motions parallel to the frontal surface within and outside of it. The balance between the hydrostatically induced pressure gradient and Coriolis forces can lead to a stationary form of geostrophic front, as first explained by Margules [5]. However, there is no theory to show that this equilibrium state is always the limiting solution for density currents that are initially not in equilibrium and whether these solutions are (a) independent of the initial condition, (b) reached in a finite period of time and distance from initial release, and (c) reached monotonically. In general one wants to know whether such a transition of density currents to a geostrophic front under the effects of rotation has universal features. Here we analyze this transition in two asymptotic regimes characterized by $\mu = ft \ll 1$ and $\mu = ft \gg 1$. One can approximate the complete picture by matching the density current solution for small values of $\mu = ft$ obtained with Taylor series expansions in a small parameter μ with that for large values of μ obtained with non-linear time averaging procedure [6–8].

The main result of this Letter is the verification of the non-linear transition curve from a non-rotating power law to a long-time solution as found in an experiment and by numerical computations.

2. Experiment

The experiments on axisymmetric rotating gravity currents were conducted in a Plexiglas tank of dimensions $75 \times 75 \times 25$ cm filled with water. The experimental apparatus is depicted in Fig. 1. A pulley system was mounted above the tank to raise a bottomless cylinder (inner radius $R_0 = 5.4$ cm, wall thickness 0.15 cm) containing dense salt water and release this water smoothly into the tank. The tank and pulley system were placed on a rotating table capable of rotating with the angular frequency $\Omega = f/2 = 1.5 \text{ s}^{-1}$. Mounted above the tank was a super-VHS video camera used to capture the fluid motion.

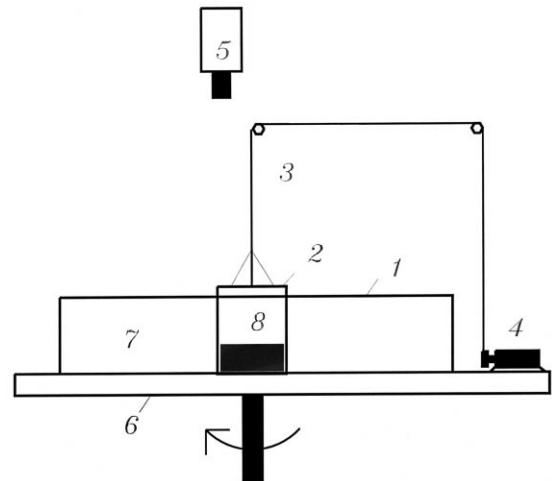


Fig. 1. Schematic of the experimental set up; (1) tank, (2) bottomless cylinder, (3) thin wire, (4) DC motor, (5) video camera, (6) rotating table, (7) distilled water, (8) salt dyed water.

The tank was filled with distilled water (depth 15 cm), and a cylinder was placed on the bottom of the tank with its center coinciding with the center of the tank. A known quantity of salt-water solution with density $\rho > \rho_0$, where ρ_0 is the tank water density, colored with dark blue thymol-blue dye, was placed inside the cylinder. Layers of salt-water solution of initial height $h_0 = 4.3$ cm and initial radius $R_0 = 5.4$ cm were used in all the laboratory experiments presented in this Letter. In experiments with rotating fluid the tank was then rotated (30–40 min), allowing the fluid to spin up to a rigid body rotation. With the camera recording, the motor was then switched on raising the cylinder and releasing the dense fluid. The experiment was then repeated but with the density of the salty fluid being half of the original value. After executing a sufficient number of runs with rotating fluids, a series of experiments was carried out with a still fluid employing the same density range as was used for rotating experiments. The position of gravity front as a function of time was recorded using a video camera and the propagation velocities of the front were determined.

2.1. Non-rotating fluid

After dense water is released from a cylinder, the flow evolved into an axisymmetric gravity current.

The front of this current propagates with a relatively large velocity from the origin and typical horizontal size (radius R) of the flow increases with time t , whereas typical vertical size (thickness h) remains approximately uniform along the radius while decreasing with time. The propagation velocity of the current dR/dt strongly depends on the excess of buoyancy Δb in the current and decreases when Δb decreases. Here $\Delta b = g\Delta\rho/\rho_0$, $\Delta\rho = \rho - \rho_0$ and g is the gravitational acceleration. Also at large values of Δb the Reynolds number, $Re = (2RdR/dt)/\nu$, is very large ($Re = 30\,000\text{--}80\,000$, ν is the kinematic viscosity of water), but only the fluid inside the current is turbulent, because of the stable buoyancy force at the upper surface of the gravity current. Visual observations showed that, except at the front in the initial stages when $ft \ll 1$, there is no significant mixing with the surrounding fluid. The flow remains stable with numerous small-scale vortices at the front. The typical horizontal size l of these vortices increases when the horizontal size R of the current increases in such a way that $l \propto R$. Neglecting mixing of the current with the surrounding fluid, the front propagation velocity in a non-rotating fluid may be scaled (this scaling follows from the balance of the horizontal pressure gradient and inertia term) as

$$dR/dt = U_F^0 = C_1(2h\Delta b)^{1/2}, \tag{1}$$

where constant C_1 is of order unity (it takes into account specific geometry of the current and bottom friction). The conservation of mass gives

$$h_0 R_0^2 = hR^2. \tag{2}$$

From (1), (2) one immediately derives the estimate

$$(R^2 - R_0^2)/R_0^2 = \frac{2C_1 t (2\Delta b h_0)^{1/2}}{R_0}. \tag{3}$$

The measured values of R for different times t in six experiments with different values of Δb were plotted in non-dimensional form and scaled, from which an estimate of $C_1 = 0.6$ was found.

2.2. Rotating fluid

After dense water is released, the initial flow pattern in a rotating fluid is approximately the same as in a non-rotating case. The flow is stable and the current has an almost axisymmetric discoid shape. With time, however, the flow behavior changes significantly, compared to a non-rotating case. The main difference is that, after a relatively short time interval, the radial propagation velocity of the front rapidly decreases and after that the horizontal size R of the current changes insignificantly. Besides this, noticeable (anti-cyclonic) azimuthal velocity arises in the flow. The results of measurements demonstrate that at moderate and small values of Δb the front velocity dR/dt rapidly drops to a small value and the flow reaches an intermediate regime. The critical size of the current at which the transition between the initial and intermediate regimes occurs depends on the value of Δb and increases when Δb increases. Neglecting again the mixing of current

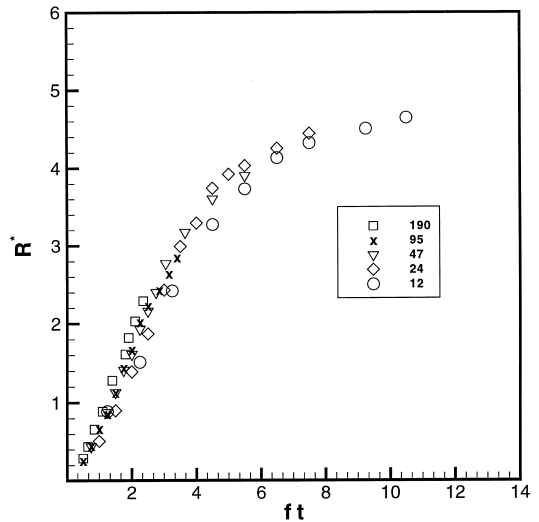


Fig. 2. Time evolution of the function R^* given by Eq. (5) for an axisymmetric gravity current in a rotating fluid ($\Omega = f/2 = 1.5 \text{ s}^{-1}$) after the release of dense fluid obtained in laboratory experiments. Different symbols are the data for different values of Δb which are given in units of cm/s^2 in a legend. The data are plotted in the non-dimensional coordinates: $R^* = f(R^2 - R_0^2)/2C_1 R_0 (2\Delta b h_0)^{1/2}$ and ft .

with the surrounding fluid, the front propagation velocity U_f^f in a rotating fluid may be scaled as

$$dR/dt = U_f^f = U_f^0 F(ft), \quad (4)$$

where U_f^0 is the front velocity in a non-rotating fluid given by (1) and $F(ft)$ is a function of ft . From (4), (2) we obtain

$$R^* = \frac{f(R^2 - R_0^2)}{2C_1 R_0 (2\Delta b h_0)^{1/2}} = \int_0^{ft} F(x) dx = \Phi(ft). \quad (5)$$

The results of measurements for five experiments with different values of Δb are given in the non-di-

mensional form in Fig. 2. The experimental data was plotted in Fig. 2 in accordance with (5). Note that since F is finite for all times, Φ continues to grow, but vary much more slowly after $t \approx f^{-1}$.

3. Numerical analysis

In this section we present numerical simulations of axisymmetric gravity currents in a rotating frame. The numerical results are compared with the experimental data presented in Section 2 (see Fig. 2).

In the present numerical study, the problem is analyzed using the shallow-water approximation. In

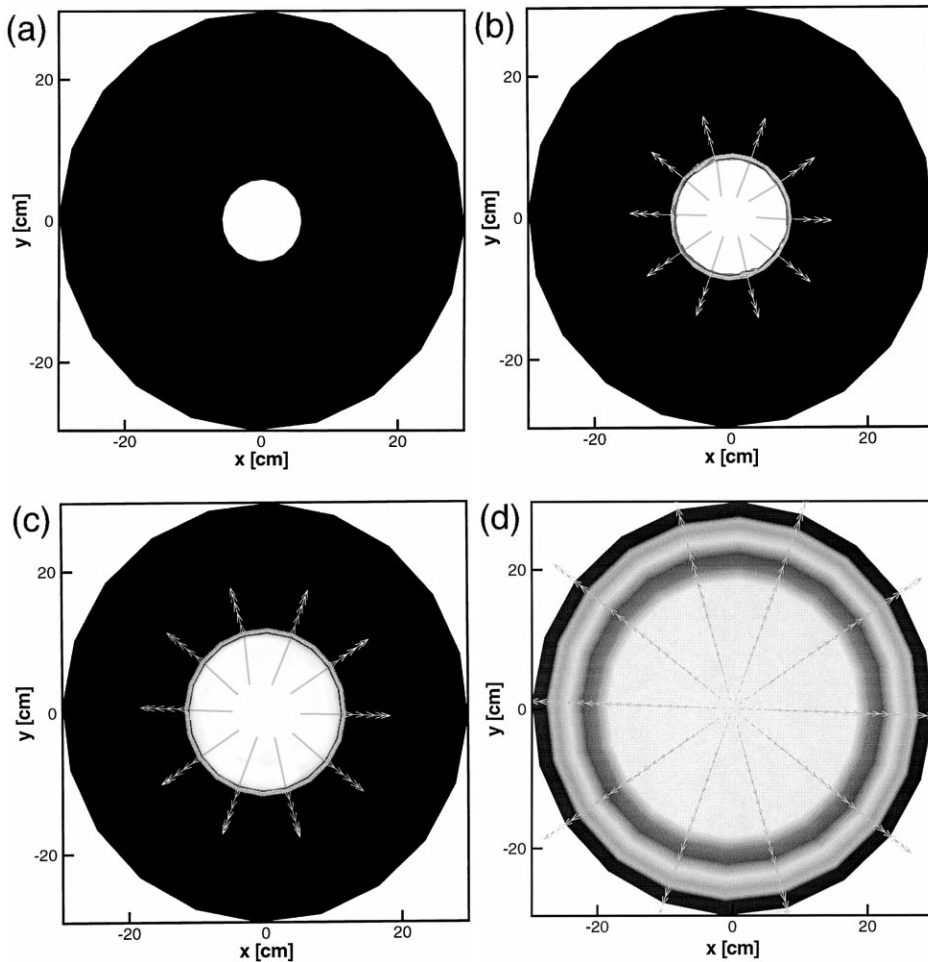


Fig. 3. Contour plots of the height and velocity vector plots of the non-rotating axisymmetric density-driven current at different times after the release of the dense fluid. Numerical conditions: $f = 0 \text{ s}^{-1}$, $\Delta b = 24 \text{ cm/s}^2$.

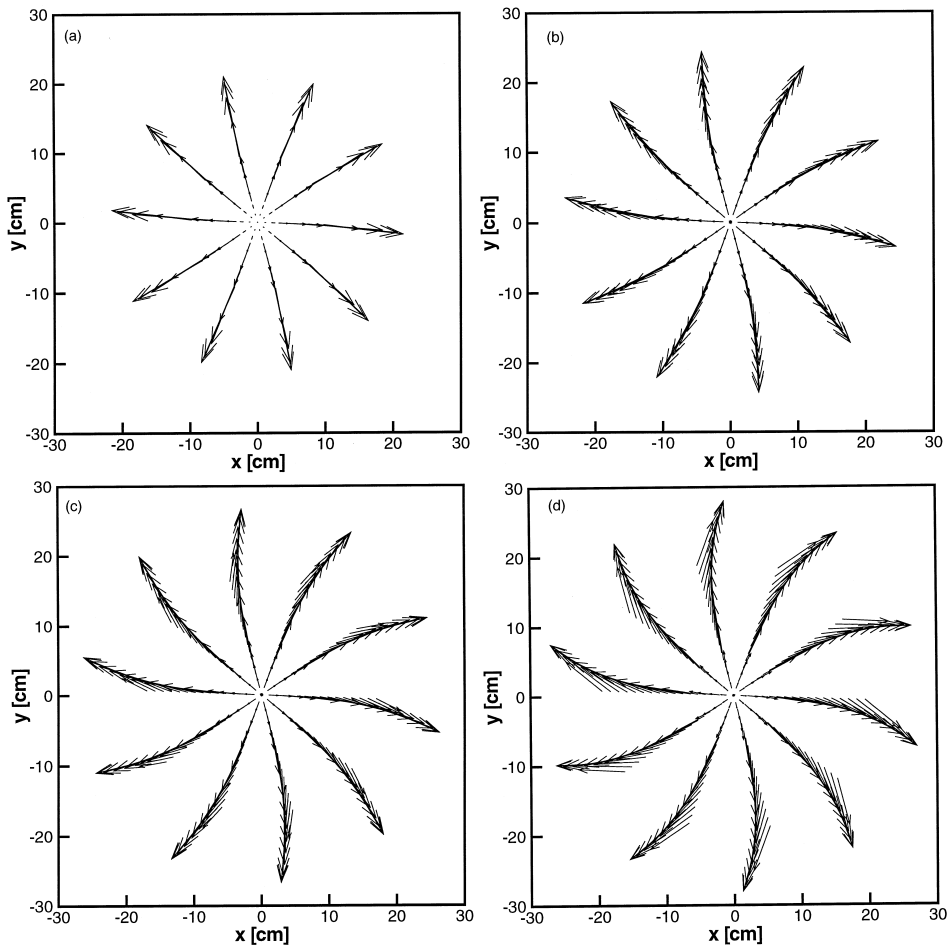


Fig. 4. Velocity vector plots of the axisymmetric density-driven current at different times after the release of the dense fluid. The numerical conditions are: $f = 3 \text{ s}^{-1}$, $\Delta b = 24 \text{ cm/s}^2$ and the background rotation is counter clockwise.

this context, the shallow-water theory has often been used to study the evolution of gravity currents. Using the shallow-water approximation, [9] obtained results in channels of rectangular cross-section. Non-rotating axisymmetric gravity currents have also been investigated in [10]. The corresponding flow in a rotating system was studied in [11,12].

The two-dimensional shallow-water equations are of the form of St. Venant equations on the f -plane which are taken as model of a shallow layer of turbulent fluid. In using these equations we assumed that: (a) fluid is incompressible; (b) the gravity current is created by the release of a liquid into an

ambient fluid; (c) vertical acceleration is negligible; (d) shear stresses effects are negligible at the free surface; (e) bottom slope is small; (f) friction losses are computed using phenomenological turbulent drag formulas. In our numerical simulations we consider only one layer of shallow fluid (heavy layer), the layer interface is assumed to be the ‘free-surface’ in our computation and shear stresses at the interface are being neglected. If we define the following depth-averaged quantities

$$U = \frac{1}{h} \int_{z_b}^{h+z_b} u \, dz, \quad V = \frac{1}{h} \int_{z_b}^{h+z_b} v \, dz \quad (6)$$

the two-dimensional depth-averaged equations of motion can be written as:

$$\frac{\partial h}{\partial t} + \nabla \cdot h\mathbf{U} = 0 \quad (7)$$

$$\begin{aligned} \frac{\partial h\mathbf{U}}{\partial t} + \mathbf{U} \cdot \nabla h\mathbf{U} = & -f\mathbf{e}_z \wedge h\mathbf{U} - \Delta b h \nabla (h + z_b) \\ & - \nabla h\mathbf{T} - \mathbf{T}_b \end{aligned} \quad (8)$$

Here h is the water depth, $\mathbf{U} = (U, V)$ represents the Cartesian depth-averaged velocity components in the x and y directions, z is the vertical direction, z_b is the bottom elevation ($z_b = 0$ in our case), $f = 2\Omega$ is the Coriolis parameter, t is the time, $\Delta b = g\Delta\rho/\rho_0$ is the reduced gravity acceleration; $\mathbf{T}_b = (\tau_{bx}, \tau_{by})$ are the bottom shear stress components and $\mathbf{T} = (T_{xx}, T_{xy}, T_{yy})$ are the depth-averaged effective stress components. In our formulation, the effective stress components are neglected and the shear stresses on the bottom surface are approximated by using the Chezy formulas

$$\tau_{bx} = \frac{\Delta b}{C^2} U(U^2 + V^2)^{1/2},$$

$$\tau_{by} = \frac{\Delta b}{C^2} V(U^2 + V^2)^{1/2},$$

where C is the Chezy constant [13].

In the numerical simulations, the governing Eqs. (7), (8) were written in conservation form. The physical domain was transformed to a rectangle by means of a mapping technique and the numerical integration was performed using an explicit finite-difference flux-splitting method [14,15]. The boundaries of the domain were kept constant during the computation.

3.1. The front condition

The effect of background rotation generates a remarkable difference in the behavior of gravity current fronts. In the non-rotating case, the front travels radially outwards at constant velocity. This velocity of the front (front condition) given by Eq. (1), has previously been studied both theoretically and experimentally. On the other hand, the velocity of the density-current front in the presence of background rotation is hindered by the Coriolis effect. In the hydrostatic analysis performed by [11], it is

assumed for simplicity that the speed of the inner's front in relation to the height was unaffected by rotation, although this is not valid when a front becomes a geostrophic front.

Our approach to the simulation of density current fronts differs from [10] and [11] in two ways. First we set the computational domain to a size large enough to contain the gravity current (the computational domain size is larger than the Rossby radius of deformation and initial condition length-scale is smaller than the Rossby radius of deformation). In this way, the density-current front never reaches the computational boundary. Second, we impose a small height (δh) extending from the location of the front to the edge of the computational boundary. Setting the computational film height in the numerical simulations is equivalent to wetting the surface in the experiment. Then, the total height h never becomes zero and imposing a condition for the velocity is not required. Typically, the computational film height was set to 0.1% of the maximum density-current height at every time step. One of the main advantages of our formulation is the capability to track the position of the front directly from the numerical simulation without imposing a front condition.

3.2. Comparison of numerical simulations with experiments

Numerical simulations are carried out with initial conditions matching the experimental parameters

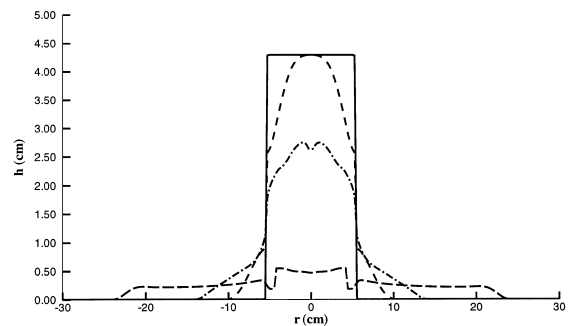


Fig. 5. Cross-section view of the axisymmetric density-driven current at different times after the release of the dense fluid. Numerical conditions: $f = 3 \text{ s}^{-1}$, $\Delta b = 24 \text{ cm/s}^2$. Horizontal axis – radius; vertical axis – height

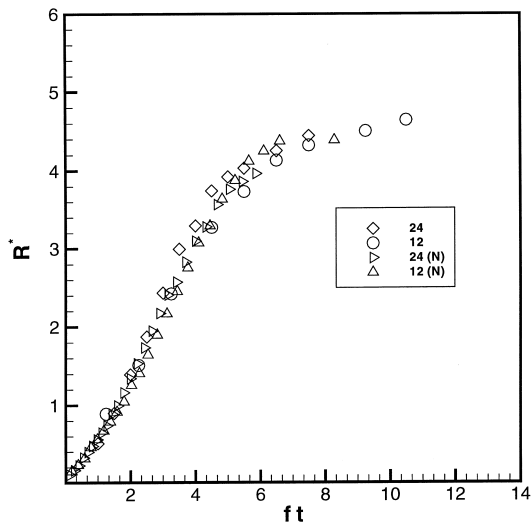


Fig. 6. Comparison with laboratory experiments for the non-dimensional function R^* as a function of the non-dimensional time ft of the axisymmetric density-driven current for different values of Δb [cm/s^2]. The legend (N) indicates numerical results.

presented in Section 2. The propagation of the axisymmetric current without rotation is shown in Fig. 3 as a function of time. The parameters chosen for the run are $\Delta b = 24 \text{ cm}/\text{s}^2$, $h_0 = 4.3 \text{ cm}$, $R_0 = 5.4 \text{ cm}$. We have chosen a circular grid layout to minimize any numerical perturbations introduced by the orientation of the grid. The speeds of propagation obtained in our simulations are scaled following the balance of horizontal pressure gradient and inertial terms through a constant C_1 described in Section 2. The value of the constant coming out from the numerical computation was found to be $C_1 = 2.8$.

The effects of background rotation on the flow are presented in Fig. 4, where the velocity field is plotted as a function of time for $f = 3 \text{ s}^{-1}$, and $\Delta b = 24 \text{ cm}/\text{s}^2$. The background rotation is clockwise causing the flow to rotate in counter clockwise direction satisfying the conservation of angular momentum. The results of experiments (described in Section 2) confirm this behavior. Fig. 5 depicts the height of the rotating density current as a function of time for the same parameters. The position of the density current front at different times for both numerical and experimental runs is plotted in non-dimensional variables

R^* versus ft in Fig. 6. The variance of the experimental data can be attributed to the uncertainty associated with the measurements of the position of the front, mixing, etc. The numerical results obtained with the shallow-water equations match the experimental data.

After an initial transient phase, the effect of rotation, for experiments and numerical simulations, is seen to slow the outward propagation of the gravity current as compared to the non-rotating case. Initially, the behavior is similar to the non-rotating case. However, after a transient time, the effect of rotation modifies the gravity current and tends to slow its radial propagation. The experimental and numerical results shown in Fig. 6 are presented for different buoyancy values. The curves are extended sufficiently long in time to demonstrate the cross-over to slower spreading in agreement with the theory [6–8].

Acknowledgements

It is here that we gratefully acknowledge the comments of Dr. K.-L. Tse and of the referees which improved the quality of the manuscript. This research was supported by the AFOSR Grant No. F49620-93-1-0172, the NSF Environmental Geochemistry and Biochemistry Initiative Grant No. 97-08452 and the Office of Vice President for Research.

References

- [1] A.E. Gill, Atmosphere–Ocean Dynamics, International Geophysics Series, vol. 30, Academic Press, 1982.
- [2] J.E. Simpson, Gravity Currents, 2nd edition, Cambridge University Press, 1997.
- [3] J.W. Rottman, J.C.R. Hunt, A. Mercer, J. Hazardous Mater. 1 (1985) 261.
- [4] Y. Noh, H.J.S. Fernando, J. Phys. Oceanogr. 23 (1993) 1142.
- [5] M. Margules, Meteorol. Z. 23 (1906) 243.
- [6] A. Mahalov, P.S. Marcus, Proc. 1st Asian Comp. Fluid Dyn. Conf. 3 (1995) 1227.
- [7] A. Babin, A. Mahalov, B. Nicolaenko, Theor. Comp. Fluid Dyn. 11 (1998) 215.
- [8] A. Babin, A. Mahalov, B. Nicolaenko, Asympt. Anal. 15 (1997) 103.

- [9] J.W. Rottman, J.E. Simpson, *J. Fluid Mech.* 135 (1983) 95.
- [10] R.T. Bonnecaze, M.A. Hallworth, H.E. Huppert, J.R. Lister, *J. Fluid Mech.* 294 (1995) 93.
- [11] M. Ungarish, H. Huppert, *J. Fluid Mech.* 362 (1998) 17.
- [12] D.A. Jones, A. Mahalov, B. Nicolaenko, *Theor. Comp. Fluid Dyn.* 13 (1999) 143.
- [13] C.B. Vreugdenhill, *Numerical Methods for Shallow-Water Flows*, Kluwer Academic Publishers, 1993.
- [14] J.R. Pacheco, A. Pacheco-Vega, *J. Fluids Eng.*, submitted.
- [15] J.R. Pacheco, Ph.D. Thesis, 1999, Arizona State University.